Low-loss and Compact Hybrid DC Circuit Breaker Scheme Using Self-commutated Semiconductor Switch Module

Lei Qi, *Member*, *CSEE*, Xinyuan Qu, Xilin Chen, Liangtao Zhan, Xiangyu Zhang, *Member*, *CSEE*, and Xiang Cui, *Fellow CSEE*, *Senior Member*, *IEEE*

Abstract—**In traditional hybrid DC circuit breakers (HCBs) schemes, complex equipment is usually required to ensure current commutation from mechanical to semiconductor switches, which cause not only additional construction costs and volume but also additional losses and maintenance work. Different from this condition, a low-loss and compact HCB scheme that does not use separate current commutation equipment is proposed in this study. By rationally using the charge and discharge of the snubber capacitor, the self-commutated semiconductor switch (SCS) module can integrate both the current commutation and shutdown functions, thereby greatly reducing cost and volume. The working process is discussed and analyzed in detail, and then a 10-kA prototype is developed and tested, which verifies the feasibility and effectiveness of the proposed scheme.**

I. INTRODUCTION

RESEARCH on DC grids has great application prospects in high voltage transmission for the past few years. Limited by low damping characteristics of a DC system, high voltage DC transmission (HVDC) requires reliable and cost-effective technology for fault cleaning. In the past 20 years, with rapid development of power electronics and multi-terminal HVDC [1]–[3], hybrid DC circuit breakers (HCBs) have been gradually used in HVDC throughout the world [4], [5]. The main advantage of HCB is that it combines the flexible controllability of semiconductor switches with superior current flow capability of mechanical switches [6].

For HCB, the key step of fault cleaning operations is the current commutation from the mechanical switch to the semiconductor switches. The basic topology of HCB is shown in Fig. 1. The auxiliary convertor represents an independent

L. Qi, X. Y. Qu, X. L. Chen, L. T. Zhan, X. Y. Zhang (corresponding author, e-mail: zhangxiangyu11@gmail.com; ORCID: https://orcid.org/0000-0002-4858-5429), X. Cui are with the State Key Laboratory of Alternate Electrical Power System with Renewable Energy Sources, North China Electric Power University, Beijing 102206, China.

structure composed of passive or active electrical components [7]–[12]. The main function of this convertor is to create conditions for commutation in case of huge fault currents.
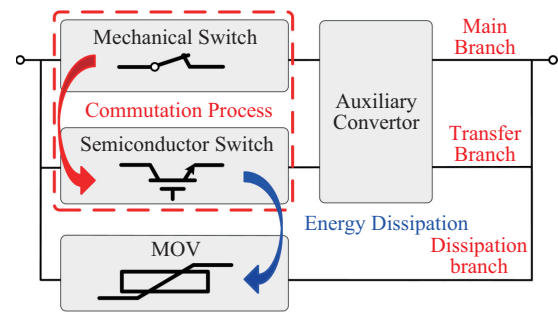

Fig. 1. Basic Topology of HCB.

Existing methods for commutation in HCB can be classified according to the cause of commutation, which can be divided into impedance pattern [13]–[15] and power pattern [16].

In the impedance pattern, the place where the fault current is generated is presented in a high impedance state in some way to promote commutation. To turn off mechanical switches, the impedance pattern is usually equipped with semiconductor switches in the main branch to realize commutation. When these semiconductor switches are turned off at the initial time, voltage can be established to promote commutation [17]. As a result, current is forced to move from the main to the transfer branch.

The other type of commutation is called power pattern, which can be described as creating an external voltage or current source to promote commutation. To force current transfer from the main branch, the power pattern usually applies an independent current or voltage source in HCB. For commutation, this type of auxiliary convertor can be placed on either the main branch or transfer branch or both [18].

For HCB in practical applications, the first issue that needs to be considered is reliability of commutation. Second, the costs of the entire equipment and available volume have to be reduced. To achieve fault cleaning, existing HCB requires a separate configuration of additional components for commutation, which causes cost, volume, reliability, and other issues.

Therefore, a low-loss and compact HCB scheme using semiconductor switches with self-commutated capability is proposed in this study. An auxiliary convertor with the function

of commutation can be integrated into a small number of modules in semiconductor switches to solve existing problems of HCB in the application and further promotion. The auxiliary convertor is only assembled on the transfer branch, while the main branch retains only mechanical switches.

The main advantage is to cancel the water-cooling system required in traditional semiconductor switches (TSS). Moreover, the two functions are integrated, that is, this auxiliary convertor not only realizes commutation but also meets the requirements of shutdown for fault current in the transfer branch. Subsequently, based on the method of power pattern, this auxiliary convertor is called the self-commutated semiconductor switch (SCS). This novel HCB scheme researched in the paper is called SCS-based HCB.

In this study, the working method of SCS and theoretical analysis of commutation is described in Chapters II and III, respectively. The 10 kA prototype and experimental verification, based on this SCS-based HCB, is introduced in the last chapter.

II. Working Method of the SCS-based HCB

In practical applications, commutation reliability is a key issue that HCB needs to solve while considering cost and volume. Additionally, an integrated method contributes to improved performance of the entire equipment. Therefore, the topology shown in Fig. 2 is evolved from the basic structure in Fig. 1, which can be classified as a power pattern for commutation.
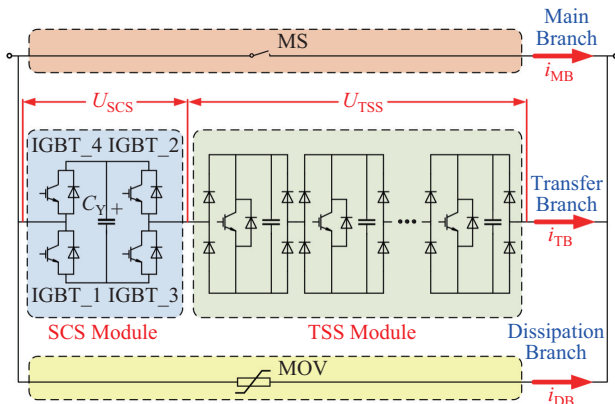

Fig. 2. Bidirectional structure of the SCS-based HCB.

The main branch is only equipped with mechanical switches, which are represented by the symbol "MS" in the following statements. The dissipation branch is composed of metal oxide varistors (MOV) [19], [20]. The main feature of the SCS is that it integrates both commutation and shutdown functions in the transfer branch. The TSS on the right can be configured with a cascaded diode bridge. TSS has multiple sub-modules connected in series. Each sub-module is composed of capacitors, IGBTs and four diodes. When IGBT is turned off, the internal capacitor can withstand transient overvoltage.

In the commutation process, the SCS module mainly realizes commutation of the fault current, and the TSS module

is responsible for conducting current of the transfer branch currently. During the shutdown process, the IGBTs in the TSS module and the SCS module turn off the fault current at the same time, and they are in series to withstand the higher transient overvoltage.

Additionally, the number of IGBTs in SCS module is more than TSS, and the price of IGBT devices is more expensive than that of diodes. Therefore, the cost of the TSS sub-module is cheaper than the SCS module. In actual engineering, in order to improve overvoltage tolerance level of the HCB, it is easily known that under the premise of meeting commutation conditions, no more SCS modules are needed, and the number of TSS sub-modules should be increased as much as possible. In Fig. 3, to describe the working method more conveniently, the current path through the TSS module is simplified.

The interior of the SCS module mainly includes a precharged capacitor represented by C_Y and insulated gate bipolar transistors (IGBT) represented by numbers IGBT_1 to IGBT_4. They are connected by symmetrical H-bridge topology, which can realize the bidirectional current flow function of the HCB.

At present, although this H-bridge topology has been maturely applied in high-power convertor technology, the SCS module shown in Fig. 2 uses a pre-charged capacitor C_Y. Both commutation and shutdown functions are integrated in HCB. Furthermore, capacitor C_Y is used to participate in the shutdown process in the transfer branch. As a result, secondary charging and recycling of energy can be realized, which is another key feature of the SCS in this study.

As shown in Fig. 3, the working process with a single direction of the SCS is mainly divided into five major stages. In Fig. 3, the parameters i_{MB}, i_{TB} and i_{DB} respectively, represent the current of the three branches mentioned in Fig. 2. Reference directions of u_{SCS} and u_{TSS} are all from left to right, and the reference direction of voltage of C_Y is from top to bottom.

In the following statements, direction of fault currents path through the main branch is from left to right by default.

Stage 1: before t_1

During this period, the main branch keeps conducting the load current and all current flows through switch MS. In the following theoretical analysis, the power side of the experimental circuit is designed as an independent reactor and a capacitor with initial power. The effect is to simulate the rising process of the load current waveform and obtain the preset fault current. During this stage, the MS will be triggered to separate at t_0.

Stage 2: t_1–t_2

The IGBT_1 and IGBT_2 will be triggered to turn on at t_1. At the same time, all IGBTs of the TSS are turned on. As shown in Fig. 2, the reference voltage direction of the capacitor C_Y is indicated in Fig. 3. As a certain amount of energy has been stored in advance, C_Y forms a path for the current flow with IGBT_1 and IGBT_2. This state also marks the beginning of the discharge process of C_Y.
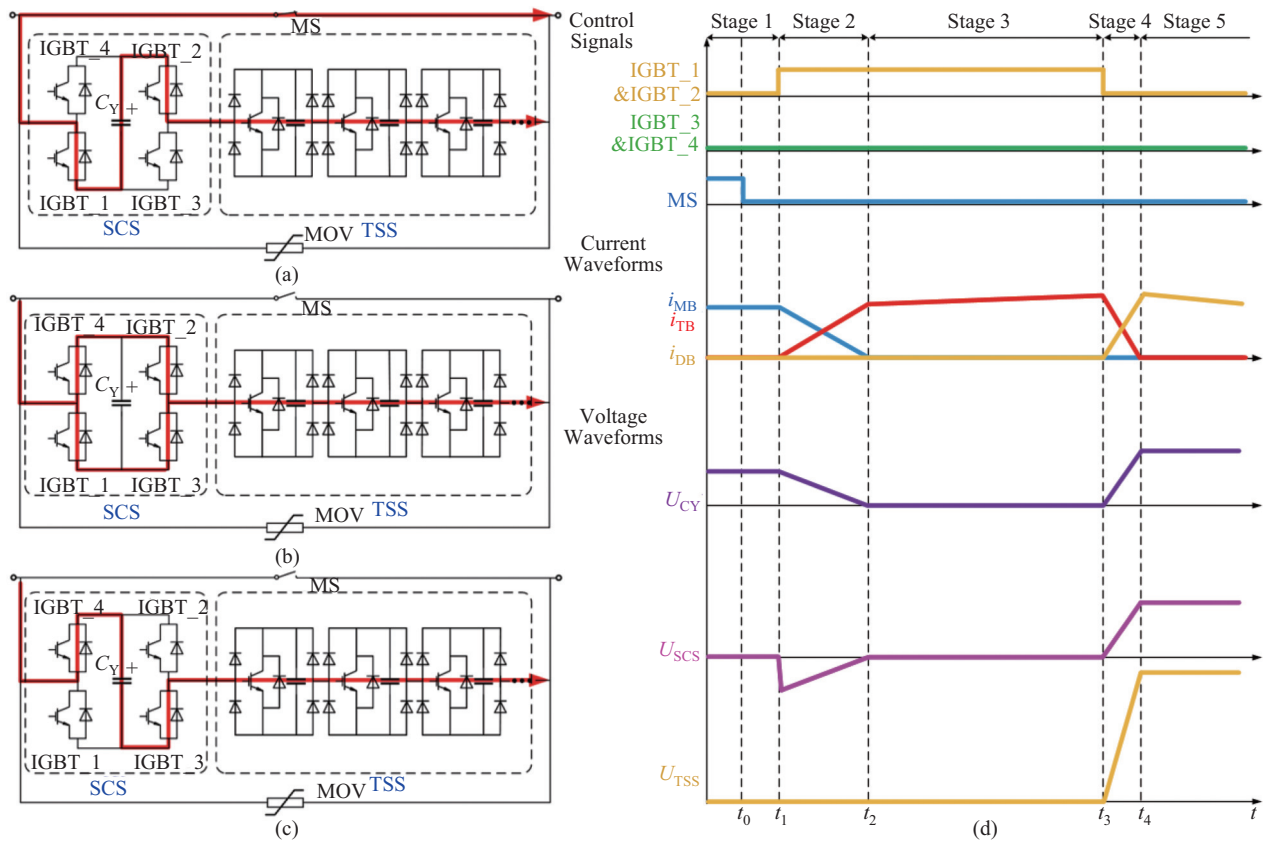
Fig. 3. Waveforms of the SCS-based HCB. (a) The initial state of commutation (t_1–t_2), (b) The final state of commutation (t_2–t_3), (c) The shutdown process of the transfer branch (after t_3), and (d) Waveforms of the SCS-based HCB in detail.

During this period, the direction of the current path through capacitor C_Y is consistent with the current direction of the MS. Thus, conditions of the power pattern are met. Furthermore, the fault current gradually transfers from the main to the transfer branch, as shown in Fig. 3(a).

This stage is the initial state of commutation and the main feature of the power pattern. Additionally, the pre-charged power of C_Y can be equivalent to an independent voltage source to force commutation.

The significant feature at this stage is that voltage and current of C_Y are increasing. Furthermore, current i_{MB} is decreasing. The sum of the two currents is equal to the initial fault current at t_1.

Stage 3: t_2–t_3

As shown in Fig. 3(b), the main process at this stage is the MS will turn off after the first zero-crossing point of the current. Generally, the pre-charged voltage of CY is designed with a certain margin to ensure reliability of commutation.

In summary, stages 2 and 3 reflect the discharge process of the pre-charged capacitor C_Y. Notably, the amount of electric energy stored in advance by C_Y does not affect the discharge speed of the C_Y. This regulation can also be further explored by adjusting the parameter configuration in the model simulation.

In addition, if the current i_{MB} has not reached the zero-crossing point after t_2, then IGBT_1 and IGBT_2 have evolved into a state connected in parallel on the transfer branch. Then,

the MS is difficult to completely turn off or break contact with an arc.

This phenomenon should be avoided in actual engineering as much as possible; otherwise, the working condition with arc breaking greatly reduces service life of the mechanical switch.

Stage 4: after t_3

This stage is specifically defined as the shutdown period of the fully controlled device in SCS. The initial moment is shown in Fig. 3(c); IGBT_1 and IGBT_2 maintain the conducting state in parallel. At a specified moment, the two IGBTs are triggered with a negative gate voltage and then turned off.

Current flows through the two freewheeling diodes in IGBT_3 and IGBT_4, and then C_Y quickly establishes a forward voltage. This process can be defined as "secondary forward charging" of C_Y, and the duration of this process is approximately microseconds.

Stage 5: after t_4

The initial moment is the current path shown in stage 4. When the forward voltage established by C_Y reaches the operating voltage of the MOV, the residual current is moved to the dissipation branch.

Stage 6: Reclosing after Stage 5

In actual operation of the power system, most of the faults are generated on overhead transmission lines, such as lightning

strikes or strong winds and other transient events. Therefore, primary equipment of the power system is usually required to perform reclosing operation. In practical applications, this type of self-recovery power supply method should also be applied, that is, it is recommended to introduce a reclosing operation after the circuit breaker breaks the fault current a single time. After one reclosing is completed, the opening command is executed. For the working conditions of the SCS-based HCB in this paper, the reclosing stage is subdivided into two modes based on the object of reclosing.

One mode involves turning on switch MS again. If fault current still exists, then it flows through the main branch again. As discussed in stage 5, C_Y has stored pre-charged voltage for the second forward charge. Therefore, the SCS can assist commutation again. When the entire circuit breaker executes an opening command, its action process repeats stages 2 to 5. Finally, capacitor C_Y still has positive charging voltage.

The other mode mainly occurs in the transfer branch. The semiconductor switches in the transfer branch are triggered to turn on again, including the IGBTs in the SCS and TSS modules. In this mode, capacitor C_Y can still be recharged in the final state.

During the charging process of C_Y, if the fault current still exists, the operation process of the SCS-based HCB will repeat the stages 3 to 5. C_Y can store the secondary forward charging voltage again, which is used to be the pre-charged voltage in the next operation.

III. ANALYSIS OF THE COMMUTATION

The specific structure and working method of SCS have been described in detail. This chapter mainly studies the commutation process.

A. Classification of Commutation Process

From discussion of stages 2 and 3 in the previous chapter, if SCS is equipped with a C_Y without a pre-charged voltage, then the MS can only be turned off under a small fault current. The principle is the same as the natural commutation method, that is, the mechanical switches use the arc voltage to move the fault current. According to the description of stages 2 and 3 in Chapter II, the evolution of these two is discussed in three cases. The TSS in Fig. 2 can be simplified into a wire during this period because the internal devices always maintain on-state. As a result, composition of the transfer branch only describes the SCS module as shown in Fig. 4.

Case 1: (I)→(II)→(IV)

The MS is turned off after the first zero crossing. Due to a certain margin of the pre-charged voltage to ensure reliable commutation, the C_Y has not been completely discharged. This is a high probability event.

Case 2: (I)→(III)

Based on description of case 1, if C_Y has been discharged before the MS is turned off, the main branch still has fault current. If the MS is still forcibly turned off at this time, then the contacts of the mechanical switch would be damaged due to a large arc. This situation is non-ideal.
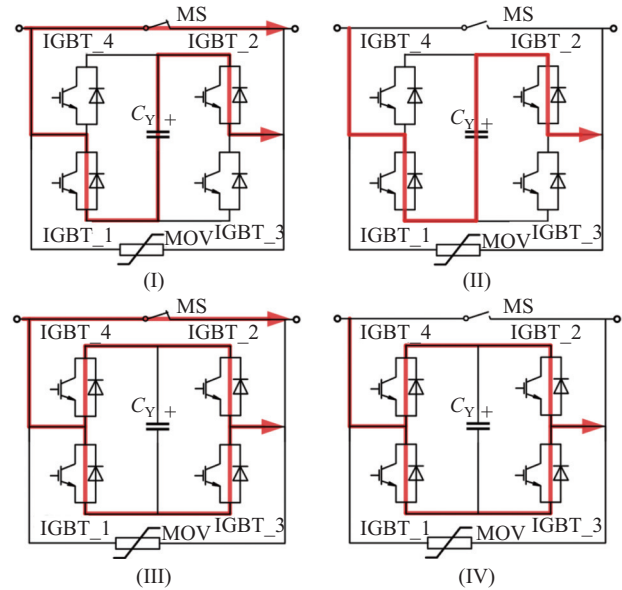

Fig. 4. Classification of commutation in SCS.

Case 3: (I)→(IV)

Combining cases 1 and 2, case 3 is the situation when the two events of turning off MS and fully discharging C_Y occur simultaneously. At this time, IGBT_1 and IGBT_2 conduct in parallel, and MS turns off. Subsequently, all fault currents flow through the transfer branch. This situation is a small probability but an ideal event.

In summary, commutation mainly focuses on the duration and reliability of the discharge process of C_Y. When the working state evolves from case 2 to 3, case 1 can be realized and situation 2 can be easily avoided by controlling the parameters, reasonably. However, configuring the parameters to achieve case 3 is difficult.

B. Mathematical Model of the SCS-based HCB

According to discussion in the previous section, to further determine the parameters to be as close as possible to case 3, a mathematical model with the voltage of C_Y as the research object can be established and studied. The transient process of commutation for the SCS module can be researched in the time domain.

The equivalent circuit between the main and transfer branches can be established according to the working method described in Chapter II. As the duration of commutation in microseconds is based on HCB, an ideal voltage source U_{DC} is used in this study to represent generation conditions of the fault current. In terms of formula derivation, U_{DC} can be equivalent to the pre-charged voltage U_{DC} stored in C_{DC}. In addition, L_L represents main loop inductance, and the total on-resistance of all devices in the TSS module is represented by R_S.

Each time point described in Fig. 5 corresponds to the time axis of Fig. 3. In stage 1, the increment of the fault current can be defined as Δi_1, and the voltage of the capacitor C_{DC} at t_1 is defined as U_1.
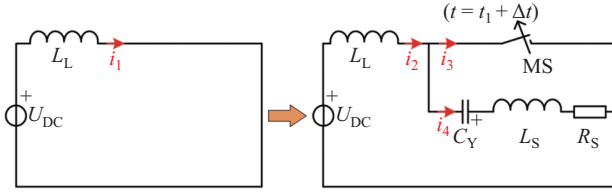
Fig. 5. Equivalent circuit of commutation.

If the pre-charged voltage is assumed to be U_{DC0} as the initial voltage at t_0, according to the law of conservation of energy, U_1 can be determined:

$$\begin{cases} \Delta U_1^2 = \Delta i_1^2 \cdot L_L/C_{DC} \\ U_1 = U_{DC0} - \Delta U_1 \\ \quad = U_{DC0} - \Delta i_1 \sqrt{L_L/C_{DC}} \end{cases} \quad (1)$$

As IGBT_1 and IGBT_2 are turned on at t_1, the current i_4 gradually increases, and total current does not change (that is, $i_1 \approx i_2$). The equation can be written as Kirchhoff's law of lumped parameter circuit:

$$U_1 + U_{CY} + R_S C_Y \frac{dU_{CY}}{dt} + L_S C_Y \frac{dU_{CY}^2}{dt^2} = 0 \quad (2)$$

Obtaining the discriminant of the equation is not difficult because it is only related to circuit parameters, such as the total stray inductance of the transfer branch (L_S) and equivalent on-resistance of the device (R_S). According to the second-order circuit expressed by the differential equation described in (2), two working conditions, namely, overdamping and underdamping, occur according to the discriminant.

However, stray inductance designed in the actual circuit structure is relatively large. Therefore, only underdamping needs to be researched. At this time, the discharge process of the capacitor presents a form of attenuated oscillation, and then the solution form of the U_{CY} is obtained as follows:

$$U_{CY}(t) = (U_{DC0} + U_1)\omega_0 e^{-\delta t} \sin(\omega t + \beta)/\omega + U_1 \quad (3)$$

p_1 and p_2 are the characteristic roots of the differential (2):

$$\begin{cases} p_1 = -\omega_0 e^{-j\beta} \\ p_2 = -\omega_0 e^{j\beta} \\ \delta = R_S/2L_S \\ \omega_0 = \sqrt{\delta^2 + \omega^2} \\ \beta = \arctan\left(\frac{\omega}{\delta}\right) \\ \omega = \sqrt{\frac{1}{L_S C_Y} - \left(\frac{R_S}{2L_S}\right)^2} \end{cases}$$

From the U_{CY} solution and component reference direction, i_4 can be determined as follows:

$$i_4(t) = -i_{CY}(t) = -\frac{dU_{CY}(t)}{dt} \quad (4)$$

We suppose that commutation time τ_H refers to the duration required from turning on the IGBT_1 and IGBT_2 to completely turning off the MS. When the i_{CY} reaches the positive peak of the first 1/4 sine wave, MS needs to be triggered to separate. From the discharge characteristics of the C_Y attenuated oscillation, τ_H can be determined:

$$\tau_H \approx \frac{\pi}{2\omega} = \pi L_S \sqrt{\frac{C_Y}{4L_S - C_Y R_S^2}} \quad (5)$$

Suppose the pre-charged voltage of capacitor C_Y is U_{CY0} before t_1. As the fault current increment is known as Δi_1, the minimum value of U_{CY0} can be determined by referring to (1), which will contribute to parameters configuration:

$$U_{CY0} \geq \Delta i_1 \sqrt{L_L/C_{DC}} \quad (6)$$

C. Characteristic Parameters of Commutation

According to theoretical analysis, the pre-charged voltage U_{CY0}, capacitance value C_Y, and time τ_H are the main parameters involved in the commutation. Equations (5) and (6) reflect two main conclusions.

After determining the value of the fault current i_1, it is necessary to determine the minimum value of the pre-charged voltage of C_Y. If the U_{CY0} is not lower than the minimum value, the MS can be successfully turned off, that is, the commutation is successful and reliable.

Second, after the circuit structure is determined, τ_H is mainly affected by the inherent parameters of the circuit. This variable needs to be adjusted according to application requirements, which will affect all the devices in the transfer branch.

In addition, by reducing the stray inductance, time τ_H can be shortened, and voltage stress of the capacitor C_Y can be reduced at the same time. Commutation time τ_H can also be shortened when capacitance of C_Y is increased. However, transient stress of the capacitor or other devices will increase.

IV. PROTOTYPE AND VERIFICATION

A. SCS-based HCB Prototype of 10 kA

According to theoretical analysis, a 10 kA SCS-based HCB prototype is developed, and the primary parameters of the prototype are determined and listed in Table I.

TABLE I
PRIMARY PARAMETERS OF THE PROTOTYPE

Parameter	Value
U_{DC}	1.6 kV
C_{DC}	20 mF
L_L	0.3 mH
C_Y	533 μF
U_{CY0}	1.0 kV
t_0 to t_1	3.0 ms
V_{on} of the diode cluster	3.6 V
I_F of the diode cluster	630 A
V_{on} of the diodes in SCS	1.3 V
I_F of the diodes in SCS	2.5 kA

The minimum value of the pre-charged voltage for capacitor C_Y can be determined by (6) in Section III.

Additionally, the diodes in SCS and diode cluster are CRRC's press-pack fast recovery diodes. The former is FYB 2000-45 and the latter is FY9 600-45. The I_F and V_{on} in Table I respectively, represent maximum conducting current and positive voltage.

Figure 6 shows the experimental circuit of the prototype. IGBT_1 and IGBT_2 remain unchanged in SCS. Only the original IGBT_3 and IGBT_4 in Fig. 2 are replaced with fast recovery diodes (D_1, D_2). As a result, the unidirectional structure studied in this manner also simplifies the configuration. As shown in Fig. 6, to reduce the number and cost of the devices used, the diode cluster is equipped with 10 press-pack diodes totally and has bidirectional current capability. In other words, the diode cluster can replace the on-resistance of the TSS module in the transfer branch as shown in Figs. 2 and 3. In addition, according to the variation of positive V-I characteristics, if current is large, the diodes can be regarded as resistors. Since the ratio of voltage to current tends to be constant. However, in this experiment, using the diode cluster to replace the TSS module is closer to a real situation. In Fig. 12, current of the diode cluster is equal to i_{TB}, which varies from 0 A to 10 kA in the initial period of commutation. Current value will vary from zero to several thousand amperes. Therefore, in this experiment, it is not recommended to replace the diode cluster with resistors.
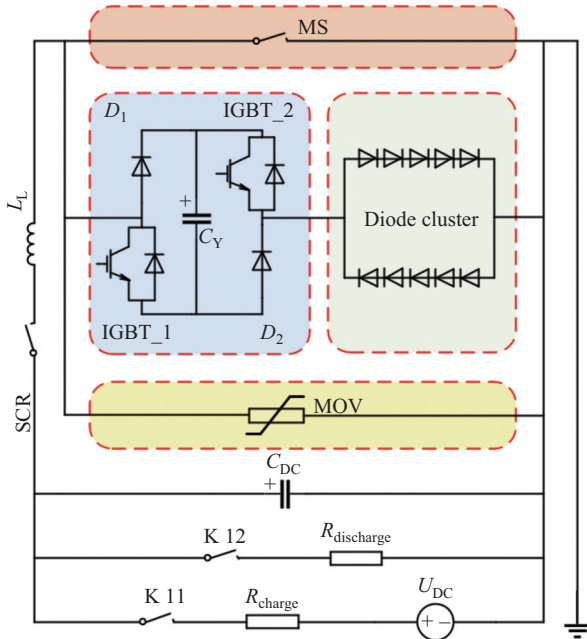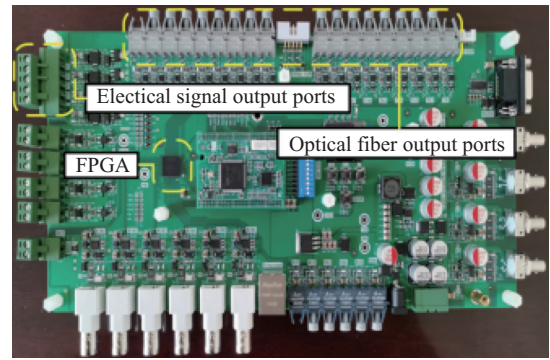

Fig. 7.   Control unit of the SCS-based HCB prototype.

fiber output ports and 4 electrical signal output ports. The former is suitable for optical fiber transmitting splicing, and the latter applies the trigger command to the MS through the optical coupler.

The operation sequence of the experimental platform and the control logic of the SCS-based HCB are depicted in Fig. 8. The content in the black frames mainly refers to the main circuit, and the content in the red frames mainly refers to the experimental circuit. In the initial stage of the experiment, both K11 and K12 are open, and the voltage of C_{DC} is equal to zero. After K11 is closed, the C_{DC} starts to charge with the help of the DSP.
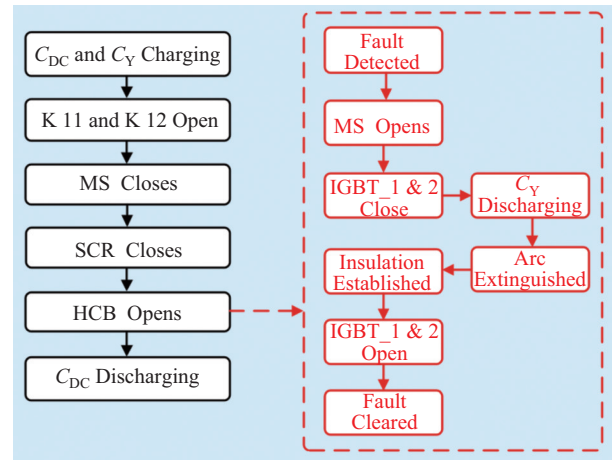

Fig. 6.   Experimental circuit of the SCS-based HCB.

Fig. 8.   The operation process of the SCS-based HCB prototype.

C_{DC} is used to generate the fault current in stage 1. The U_{DC} in Fig. 6 represents the charging power supply. In Fig. 10(a), it mainly uses a dedicated DSP to charge the experimental capacitor C_{DC}, which converts the alternating voltage of 220 V to DC voltage. The two branches at the bottom of Fig. 6 are respectively, for charging and discharging the capacitor C_{DC}. R_{charge} and $R_{discharge}$ are respectively represented as charge resistor and discharge resistor of C_{DC}, and they are controlled by other mechanical switches.

The control sequence of IGBT_1, IGBT_2 and MS has been described in Fig. 3(d). During the experiment, it can be realized by software through FPGA as shown in Fig. 7. The control program has been stored in the FPGA before the experiment. The whole PCB board is equipped with 18 optical

When the C_{DC} charging voltage exceeds the preset voltage U_{CY0}, the switch K11 is closed. Subsequently, the SCR is triggered to conduct after the MS opens, and C_Y starts charging at this time. It should be noted the operation sequence is mainly involved in the SCS module. The control requirements of the MS and IGBTs have been described in Fig. 3(d). Finally, capacitor C_{DC} can achieve the discharge by closing K12.

In order to show details of the prototype more clearly, the mechanical structures for SCS are shown in Fig. 9. The direction of current through the SCS module has been identified in Fig. 9(a). Compared with Fig. 6, connection between the diodes and the IGBTs can be recognized from Fig. 9(b).

The prototype entity shown in Fig. 10 corresponds to the experimental circuit in Fig. 6, which mainly includes the main
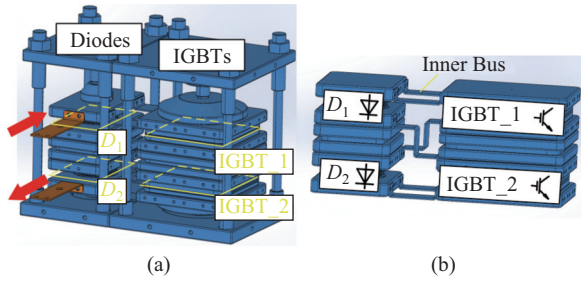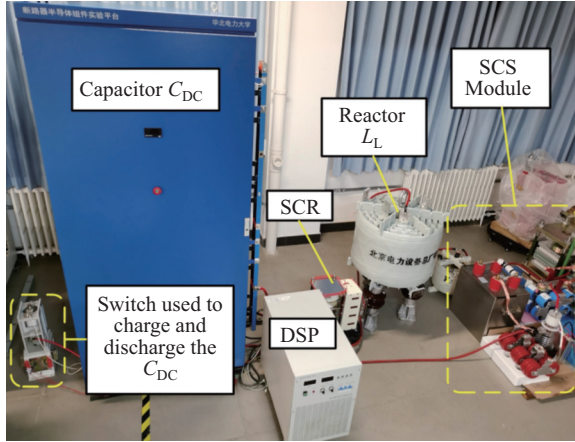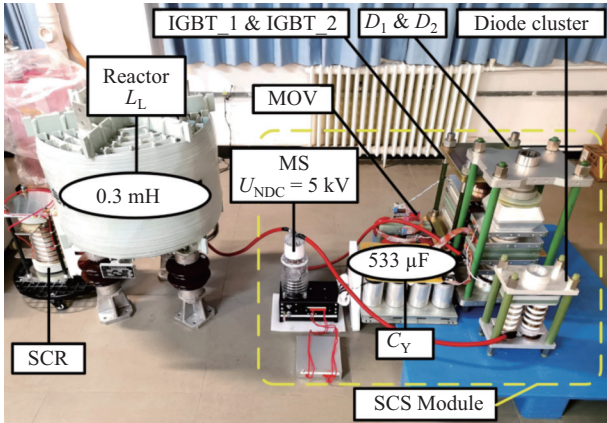
Fig. 9. Mechanical structures based on the pressure mechanism. (a) Mechanical structures in SCS (C_Y is hidden), and (b) connection details of diodes and IGBTs.

Fig. 10. Overview of the experimental prototype. (a) Composition of the prototype. (b) Details of the prototype.

circuit and experimental circuit. The main circuit is composed of the experimental capacitor charge and discharge circuit, main circuit reactor L_L and SCR. The experimental circuit is mainly composed of the SCS module.

The main circuit mainly represents the generation of fault current. The IGBTs and diodes in the TSS module are assembled with structures based on the pressure mechanism. The former uses ABB's press-pack IGBT devices, and the latter uses CRRC's press-pack fast recovery diodes (FYB2000-45).

C_Y is composed of 12 capacitors, which are assembled in the form of four capacitors in parallel and then three groups

in series. The single capacitance value of these capacitors is 400 μF. A single capacitor has a rated DC voltage of 1.1 kV and transient voltage of 3 kV. Additionally, C_Y is equipped with a megohm-level discharge resistor. In order to make voltage U_{CY0} controllable in the next experiment, the discharge resistor for C_Y in Fig. 11 is used to exhaust the energy which was obtained by the secondary forward charging. In fact, it's unnecessary to configure a discharge resistor for C_Y in practical engineering. The secondary charging voltage can be used in the next operation of the SCS-based HCB, which realizes system energy recycling.
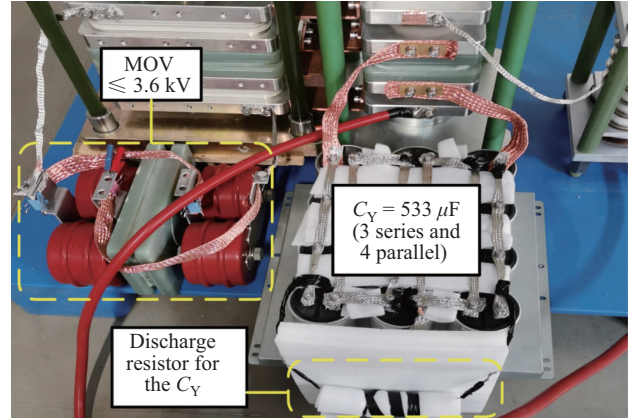

Fig. 11. Configuration of pre-charged capacitor C_Y.

B. Verification of the Experimental Prototype

Based on the experimental prototype, it is verified that current level of the prototype reaches 10 kA.

Stray inductance in the transfer branch is extracted at approximately 1 μH based on previous simulations. Therefore, the τH can be estimated to be approximately 36 μs after the primary parameters of the prototype have been determined. In the actual prototype experiment, τH is measured to be approximately 50 μs as described in Fig. 12(a). Minimal error is observed between the measured and calculated values.

As shown in Fig. 12(b), C_Y starts to discharge, and voltage of MS drops slightly at 7.4 ms. As the main branch is only equipped with MS and is connected in parallel with the transfer branch, voltage on the MS is almost equal to zero.

Results verify the prototype can realize commutation within 50 μs, which can confirm the effectiveness of the commutation strategy in this study.

Figure 13 shows three groups of experimental results of the pre-charged voltage of C_Y and commutation time under different fault currents. In the commutation process, the initial current values of the three groups are 2 kA, 6 kA and 9.7 kA, and the commutation time are 16 μs, 25 μs and 48 μs, respectively. Pre-charged voltages of capacitor C_Y are 450 V, 750 V and 970 V, respectively. At $t_3 = 7.89$ ms, the semiconductor switches in SCS and TSS modules are closed simultaneously. Subsequently, C_Y starts to be recharged. Charging currents in the three groups are 1.9 kA, 6.0 kA and 10.3 kA.

In the current waveforms of group C, the green curve is hypothetical. It is only to represent the surplus energy of capacitor C_Y. Reliability of successful commutation in SCS
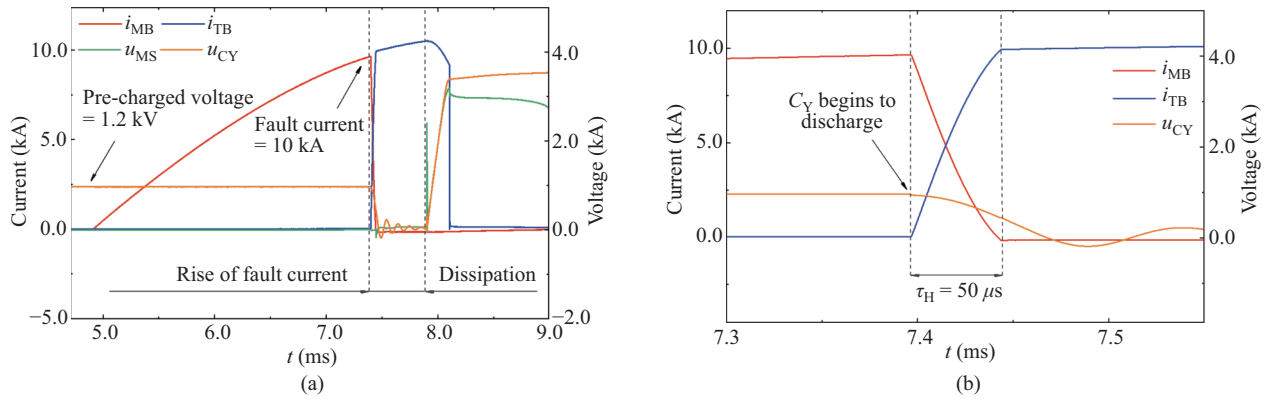
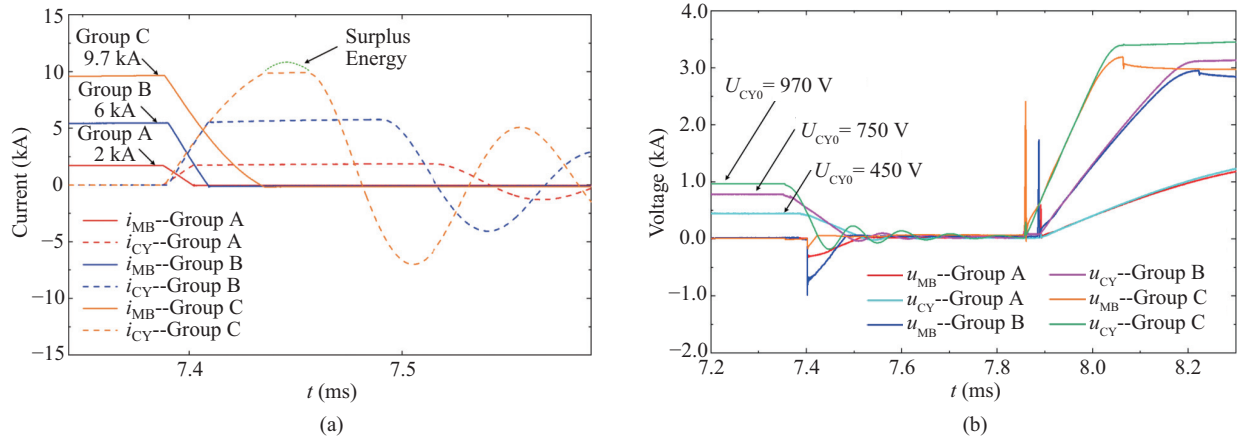Fig. 12.   Verification of the prototype. (a) Experimental results of 10 kA. (b) Waveforms of Commutation.

Fig. 13.   3 groups of experimental results. (a) Current waveforms during commutation (t_1–t_2). (b) Voltage waveforms (t_0–t_4).

module improves with increase of surplus energy. According to (6) and Table I, the minimum value of U_{CY0} is calculated. In the experimental prototype, U_{CY0} should increase a certain margin based on the calculated value to ensure commutation reliability. In each group of experiments, the discharge current of C_Y does not reach the first sinusoidal peak, and the current of C_Y is equal to the fault current. In this way, i_{MB} is sufficient to be commutated to the transfer branch. The main parameters in each group of experiments have been shown in Table II.

TABLE II
MAIN EXPERIMENTAL RESULTS OF THREE GROUPS

Number	Parameter	Value
Group A	U_{DC0}	0.3 kV
	U_{CY0}	0.45 kV
	τ_H	16 μs
	i_{MB} at t_1	2 kA
	u_{CY} after t_4	3.4 kV
Group B	U_{DC0}	0.9 kV
	U_{CY0}	0.75 kV
	τ_H	25 μs
	i_{MB} at t_1	6 kA
	u_{CY} after t_4	3.2 kV
Group C	U_{DC0}	1.6 kV
	U_{CY0}	0.97 kV
	τ_H	48 μs
	i_{MB} at t_1	9.7 kA
	u_{CY} after t_4	1.3 kV

In addition, the effect of energy recycling can be seen from Fig. 13(b). Taking group C as an example, the secondary charging voltage of C_Y almost reaches a constant value at $t_4 = 8.05$ ms, which can be regarded as the pre-charged voltage of C_Y in the next HCB operation.

V. CONCLUSION

SCS-based HCB and experimental prototypes have been studied. Theoretical analysis and experimental results based on the prototype are formed into the following conclusions.

The SCS module integrates commutation and shutdown functions for a fault current without using separate current commutation equipment, which is the main feature of the SCS-based HCB described in this study. Furthermore, C_Y is not only used as a snubber capacitor for the SCS module, but also can be recharged in the process of shutdown. As a result, by rationally using the charge and discharge, energy in C_Y can be recycled in practical applications, thereby greatly reducing cost and volume. Based on the experimental prototype, results show the duration of commutation is approximately 50 μs. The SCS-based HCB proposed in this paper is verified to be feasible and effective.

REFERENCES

[1] H. Rao, "Architecture of Nan'ao multi-terminal VSC-HVDC system and its multi-functional control," *CSEE Journal of Power and Energy*

Systems, vol. 1, no. 1, pp. 9–18, Mar. 2015.

[2] Y. B. Shu and W. J. Chen, "Research and application of UHV power transmission in China," *High Voltage*, vol. 3, no. 1, pp. 1–13, Mar. 2018.

[3] V. C. Billon, J. P. Taisne, V. Arcidiacono, and F. Mazzoldi, "The Corsican tapping: from design to commissioning tests of the third terminal of the Sardinia-Corsica-Italy HVDC," *IEEE Transactions on Power Delivery*, vol. 4, no. 1, pp. 794–799, Jan. 1989.

[4] X. Y. Zhang, Z. Q. Yu, R. Zeng, M. Zhang, Y. H. Zhang, F. L. Xiao, and W. Li, "HV isolated power supply system for complex multiple electrical potential equipment in 500 kV hybrid DC breaker," *High Voltage*, vol. 5, no. 4, pp. 425–433, Aug. 2020.

[5] N. Flourentzou, V. G. Agelidis, and G. D. Demetriades, "VSC-based HVDC power transmission systems: an overview," *IEEE Transactions on Power Electronics*, vol. 24, no. 3, pp. 592–602, Mar. 2009.

[6] W. J. Wen, Y. L. Huang, Y. S. Sun, J. H. Wu, M. Al-Dweikat, and W. D. Liu, "Research on current commutation measures for hybrid DC circuit breakers," *IEEE Transactions on Power Delivery*, vol. 31, no. 4, pp. 1456–1463, Aug. 2016.

[7] Z. Dongye, L. Qi, B. Ji, X. Wei and X. Cui, "Circuit Model with Current Interruption for Hybrid High Voltage DC Circuit Breakers to Achieve Precise Current Experiments," *CSEE Journal of Power and Energy Systems*, vol. 8, no. 4, pp. 1250–1260, Jul. 2022.

[8] S. Tokoyoda, T. Inagaki, F. Page, M. Sato, K. Kamei, M. Miyashita, and H. Ito, "Interruption characteristics of vacuum circuit breaker and the application to DCCB," in *13th IET International Conference on AC and DC Power Transmission (ACDC 2017)*, Manchester, UK, 2017.

[9] W. X. Sima, Z. Z. Fu, M. Yang, T. Yuan, P. T. Sun, X. Han, and Y. Si, "A novel active mechanical HVDC breaker with consecutive interruption capability for fault clearances in MMC-HVDC systems," *IEEE Transactions on Industrial Electronics*, vol. 66, no. 9, pp. 6979–6989, Sep. 2019.

[10] M. Abdolkarimzadeh, M. Nazari-Heris, M. Abapour, and M. Sabahi, "A bridge-type fault current limiter for energy management of AC/DC Microgrids," *IEEE Transactions on Power Electronics*, vol. 32, no. 12, pp. 9043–9050, Dec. 2017.

[11] A. Heidary, H. Radmanesh, K. Rouzbehi, and J. Pou, "A DC-reactor-based solid-state fault current limiter for HVdc applications," *IEEE Transactions on Power Delivery*, vol. 34, no. 2, pp. 720–728, Apr. 2019.

[12] B. Yin, X. Zeng, J. F. Eastham, D. Vilchis-Rodriguez and X. Pei, "Novel fast operating moving coil actuator with compensation coil for HVDC circuit breakers," CSEE Journal of Power and Energy Systems, vol. 7, no. 5, pp. 1041–1050, Sept. 2021.

[13] R. Majumder, S. Auddy, B. Berggren, G. Velotto, P. Barupati, and T. U. Jonsson, "An alternative method to build DC switchyard with hybrid DC breaker for DC grid," *IEEE Transactions on Power Delivery*, vol. 32, no. 2, pp. 713–722, Apr. 2017.

[14] Z. Chu, B. Xu, Z. Q. Yu, and N. H. Wang, "Research on topological structure and simulation of hybrid DC circuit breaker," *The Journal of Engineering*, vol. 2019, no. 16, pp. 3310–3314, Mar. 2019.

[15] M. Ahmad and Z. X. Wang, "A hybrid DC circuit breaker with fault-current-limiting capability for VSC-HVDC transmission system," *Energies*, vol. 12, no. 12, pp. 2388, Jun. 2019.

[16] X. Y. Zhang, Z. Q. Yu, R. Zeng, Y. L. Huang, B. Zhao, Z. Y. Chen, and Y. M. Yang, "A state-of-the-art 500-kV hybrid circuit breaker for a DC grid: the world's largest capacity high-voltage DC circuit breaker," *IEEE Industrial Electronics Magazine*, vol. 14, no. 2, pp. 15–27, Jun. 2020.

[17] L. Novello, F. Baldo, A. Ferro, A. Maistrello, and E. Gaio, "Development and testing of a 10-kA hybrid mechanical–static DC circuit breaker," *IEEE Transactions on Applied Superconductivity*, vol. 21, no. 6, pp. 3621–3627, Dec. 2011.

[18] A. Shukla and G. D. Demetriades, "A survey on hybrid circuit-breaker topologies," *IEEE Transactions on Power Delivery*, vol. 30, no. 2, pp. 627–641, Apr. 2015.

[19] K. Raju and V. Prasad, "Modelling and validation of metal oxide surge arrester for very fast transients," *High Voltage*, vol. 3, no. 2, pp. 147–153, Jun. 2018.

[20] X. Y. Zhang, Z. Q. Yu, Z. Y. Chen, Y. L. Huang, B. Zhao, and R. Zeng, "Modular design methodology of DC breaker based on discrete metal oxide varistors with series power electronic devices for HVDC application," *IEEE Transactions on Industrial Electronics*, vol. 66, no. 10, pp. 7653–7662, Oct. 2019.

Lei Qi received the B.S., M.S., and Ph.D. degrees in Electrical Engineering from North China Electric Power University, Baoding, China, in 2000, 2003, and 2006, respectively. He is currently a Professor of Electrical Engineering at North China Electric Power University. His research interests include electromagnetic fields theory and application, electromagnetic compatibility in power systems, and advanced power transmission technology.

Xinyuan Qu received a B.S. degree in 2019, from Hefei University of Technology, Anhui, China. He is currently working toward an M.S. degree in Electrical Engineering in North China Electric Power University, Beijing, China. He is working on improving performance of semiconductor switches and researching new power system protection equipment. His research interests include application of high-power semiconductor switches and advanced power transmission.

Xilin Chen received a B.S. degree in 2019, from North China Electric Power University, Beijing, China, where she is currently working toward an M.S. degree, both in Electrical Engineering. She is currently working on DC circuit breakers in medium and high-voltage DC grids. Her research interests include application of wide band-gap devices, electromagnetic compatibility in power systems, advanced power transmission.

Liangtao Zhan received a B.S. degree in 2020, from Zhejiang University of Technology, Hangzhou, China. He is currently working toward an M.S. degree in Electrical Engineering in North China Electric Power University. His main research direction is to improve turn-off capacity of power electronic switches.

Xiangyu Zhang received B.S. and Ph.D. degrees in Electrical Engineering from the Department of Electrical Engineering, Tsinghua University, Beijing, China, in 2015, and 2020, respectively. He is currently a Lecturer of Electrical Engineering at North China Electric Power University. His current research interests include HVDC systems and direct current circuit breakers.

Xiang Cui (M'97–SM'98) received a B.Sc. degree from North China Electric Power University, Baoding, China, in 1982, and a M.Sc. degree from North China Electric Power University, Beijing, China, in 1984, both in Electrical Engineering, and a Ph.D. degree in Accelerator Physics from China Institute of Atomic Energy, Beijing, China, in 1988.

He is currently a Professor and Vice Director of the State Key Laboratory of Alternate Electrical Power System with Renewable Energy Sources, North China Electric Power University, Beijing. His research interests include computational electromagnetics, electromagnetic environments and electromagnetic compatibility in power systems, insulation and magnetic problems in high-voltage apparatuses. Prof. Cui is a Standing Council Member of the China Electro Technical Society, a Fellow of IET, and a Senior Member of IEEE. He is also an Associate Editor of IEEE Transactions on Electromagnetic Compatibility.